analytical chemistry

Article

Cite This: Anal. Chem. 2019, 91, 6149−6154

pubs.acs.org/ac

Switchable Nanochannel Biosensor for H_2S Detection Based on an Azide Reduction Reaction Controlled BSA Aggregation

Ruiping Zhang,[†,+] Xiaoya Chen,[‡,+] Zhongyue Sun,[‡,+] Sen Chen,[‡] Jing Gao,[#] Yao Sun,[*,‡] and Haibing Li[*,‡]

[†]The Affiliated Cancer Hospital of Shanxi Medical University, Imaging Department of Shanxi Medical University, Taiyuan 030001, China

[‡]Key laboratory of Pesticides and Chemical Biology, Ministry of Education, International Joint Research Center for Intelligent Biosensor Technology and Health, Center of Chemical Biology, College of Chemistry, Central China Normal University, Wuhan 430079, China

[#]Jiangsu Key Laboratory of Medical Optics, Suzhou Institute of Biomedical Engineering and Technology, Chinese Academy of Sciences, Suzhou 215163, China

Supporting Information

ABSTRACT: Hydrogen sulfide (H_2S) is the third endogenous gaseous signal molecule in organisms that can directly increase the salt tolerance of plants by closing the K^+ channel. Inspired by the important role of H_2S in nature, we have designed a H_2S-responsive artificial nanochannel biosensor based on an azide reduction reaction strategy. This biomimetic device demonstrates an excellent H_2S selective response owing to specific azide reduction by H_2S inducing BSA aggregation on the channel with a high ion gating ratio. Furthermore, this H_2S-responsive biosensor shows excellent reversibility and stability and a fast response rate, which will help us better understand the synergistic effect of H_2S messengers in the ion channels of living organisms.

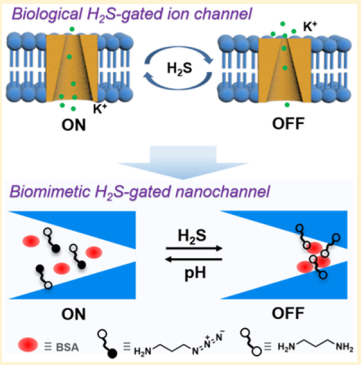

Hydrogen sulfide (H_2S) has long been known as a toxic gas and environmental hazard, however, recent studies have indicated the important biological roles of H_2S as the third endogenous mediator after nitric oxide (NO) and carbon monoxide (CO).[1−4] H_2S is involved in a wide range of physiological and pathological activities, including blood flow regulation, inflammatory reactions modulation, and the immune system stabilization.[5−7] Furthermore, H_2S has gained increasing attention from plant researchers owing to its association with adaptive responses against multiple stress conditions.[8,9] For example, H_2S inhibits K^+ transport through channels on the plasma membrane to increase the salt tolerance of plants.[9] Considering the significant role of H_2S in living systems, constructing a H_2S-responsive nanochannel biosensor in vitro will help us to better understand the mechanism of H_2S physiological functions. However, the instability and fragility of the embedded lipid bilayers makes their application in real environments difficult, restricting their practical applications.[10−15]

Fortunately, artificial nanochannels are a promising platform for mimicking various biological processes in vitro because of their greater size flexibility and robust chemical and mechanical properties.[16−24] Similar to biological channels, these biomimetic nanochannels have been shown to display transport properties, such as ion selectivity, current rectification, and ion gating, by controlling the surface properties of the pore walls.[25−31] To realize a specific response to diverse environmental stimuli, the channel surface is modified with various functional molecules, thus, facilitating research scientists to develop various smart nanochannels.[32−36] Despite significant progress, some issues still need to be addressed. For example, the nanochannel properties are not always very stable after modification and precisely controlling the ratio of effective modification on nanochannels is still a nontrivial task.[37−40] Therefore, the development of simple and straightforward strategies for endowing smart to artificial nanochannel biosensors in response to gas molecule is urgently required.

Inspired by the H_2S-responsive channel in nature, we have designed an artificial H_2S-responsive biosensor based on label-free nanochannels by adding a mixture of azido-propylamine (AP) and bovine serum albumin (BSA) to the solution to achieve highly selective and reversible H_2S recognition (Figure 1). Taking advantage of the known unique reduction of azido groups to amine groups by H_2S,[41,42] AP can be readily reduced to 1,3-diaminopropane (DP) in the presence of H_2S. The reduced amine group of DP can then interact with the carboxyl

Received: February 10, 2019
Accepted: April 1, 2019
Published: April 1, 2019

DOI: 10.1021/acs.analchem.9b00752
Anal. Chem. 2019, 91, 6149−6154

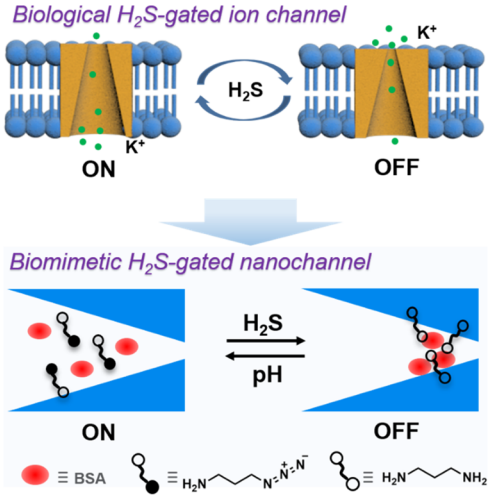

Figure 1. Schematic of the design of a biomimetic H_2S-responsive nanochannel biosensor using an azide reduction reaction controlled BSA aggregation.

groups ($-COO^-$) of BSA (pI, 4.8), forming DP/BSA ion pairs at pH 7.0. It changes the charge of BSA, causing the formation of BSA aggregates in the channel and the absorption of DP/BSA complex on the channel surface, which inhibits the K^+ transportation activity (OFF state). Meanwhile, the K^+ transportation ability was readily recovered (ON state) by changing the pH to base conditions (pH 10), which might be attributed to dissociation process of DP/BSA complexes. Therefore, this H_2S-responsive biosensor is simple, requires no external modification, and exhibits a highly specific and sensitive H_2S response in complex matrices without interference. Furthermore, the H_2S-responsive biosensor also exhibits excellent reversibility and stability based on controlled BSA aggregation, which indicates its efficiency and reusability for real-world applications.

EXPERIMENTAL SECTION

Fabrication of Nanochannel. A nanochannel was prepared in PET film using the ion-track-etching technique (see Figure S6). Before the etching process, each side of the PET membrane was exposed in UV light (365 nm) for 1 h. To produce a single conical nanochannel, the first etching was performed from one side. The PET membrane was embedded between the two chambers of a conductivity cell; one chamber was filled with etching solution (9 M NaOH), and the other chamber was filled with stopping solution (1 M KCl + 1 M HCOOH). Then, a voltage of 1 V was applied across the membrane to monitor the etching process (20 min at 35 °C). When the current value reached 2.5 nA, stopping solution (1 M KCl + 1 M HCOOH) was added on both sides of the membrane for 20 min. A second etching carried out at 25 °C (adding etching solution 1 M NaOH) into both sides. After about 2 h, when the transmembrane current reached 50 nA, stopping solution was added. The diameter of the large opening of the conical nanochannel, which was called base (D), was determined by scanning electron microscopy (SEM) to be about 480 nm, and the diameter of the small opening, which was called the tip (d_{tip}), was estimated mathematically to be about 29 nm.

Ion Current Measurement. Ion currents were measured with a Keithley 6487 picoammeter (Keithley Instruments, Cleveland, OH). Ag/AgCl electrodes were used to apply a transmembrane potential across the film. The film was mounted between the two halves of the conductance cell. To record the $I-V$ curves, a scanning triangle voltage signal from −2 V to +2 V with a 40 s period was selected. Each test was repeated 5 times to obtain the average current value at different voltages.

Contact Angle Measurement. Contact angles were measured using a contact-angle system at room temperature and saturated humidity. Contact angle data was also used to confirm the reaction. We immersed the PET membrane in the presence of the BSA, BSA/AP, BSA/H_2S, and BSA/AP/H_2S solution, and then, we measured the contact angle. Under neutral conditions, both the BSA and membrane are negatively charged, and under electrostatic repulsion, BSA has no interaction with the membrane effect. After the membrane was modified with a mixture of BSA/AP/H_2S, because the positively charged production of amine group interacts with the negatively charged BSA, it was positively charged to further increase the surface interaction with the negatively charged membrane.

SEM Characterization. The diameter of the base was estimated from the multitrack membrane by field-emission scanning electron microscopy (FESEM), which was etched under the same conditions as the single-channel sample. In this work, before modification, the base diameter was about 480 nm, and the tip diameter was estimated to be about 29 nm.

Infrared Spectra Measurement. Infrared spectra were measured by an infrared spectrometer. We prepared BSA, BSA/H_2S, BSA/AP, and BSA/AP/H_2S. The disappearance of the azide peak at 2130 cm^{-1} in the BSA/AP/H_2S system indicated that the azide in the BSA/AP/H_2S system was reduced to amine by H_2S.

Zeta-Potential Measurement. Zeta-potential were measured using a zeta potential analyzer (Malvern Zetasizer Nano ZS90). Zeta-potential indirectly reflects the type of charge and the amount of electricity of the surface of particle. Considering the difficulty of measuring the zeta-potential of PET membrane, herein, we measured the zeta-potential of BSA, BSA/AP, BSA/H_2S, and BSA/AP/H_2S systems in the solution phase. In this study, the azide can be reduced into free amine (strong positive charge) by H_2S. Therefore, the COO^- group of BSA could interacted with the free amine group, which lead to greatly reduce the negative charge of BSA.

H_2S-Response Nanochannel Biosensor for Complex Matrices. First, the actual water sample was collected from the Yangtze River should be pretreated. First, BSA (0.25 mg/mL) and 5×10^{-5} M AP were mixed together, and then, 10^{-4} M F^-, Cl^-, Br^-, I^-, OAC^-, NO_2^-, HCO_3^-, HSO_3^-, SO_4^{2-}, ClO_4^-, and citrate solution were added into the system. We measure the performance of nanochannel by $I-V$ curve joining different concentrations of AP and H_2S in the reaction liquid mixed with BSA by using actual samples under the same conditions.

Finite-Element Computation. To investigate the gating mechanism of the NO-responsive nanochannel biosensor, finite-element computations based on the Poisson and Nernst−Planck equations were performed using COMSOL Multiphysics 5.3. The diffusion coefficients of the cations and anions in bulk solution were 2.0×10^{-9} m^2/s (K^+ and Cl^-). The total length of the simulated models was uniformly set to 12 μm. Two models with isopycnic opposite charges were prepared to simulate the ON and OFF states of the NO-responsive biosensor. It is obvious that rather larger

DOI: 10.1021/acs.analchem.9b00752
Anal. Chem. 2019, 91, 6149−6154

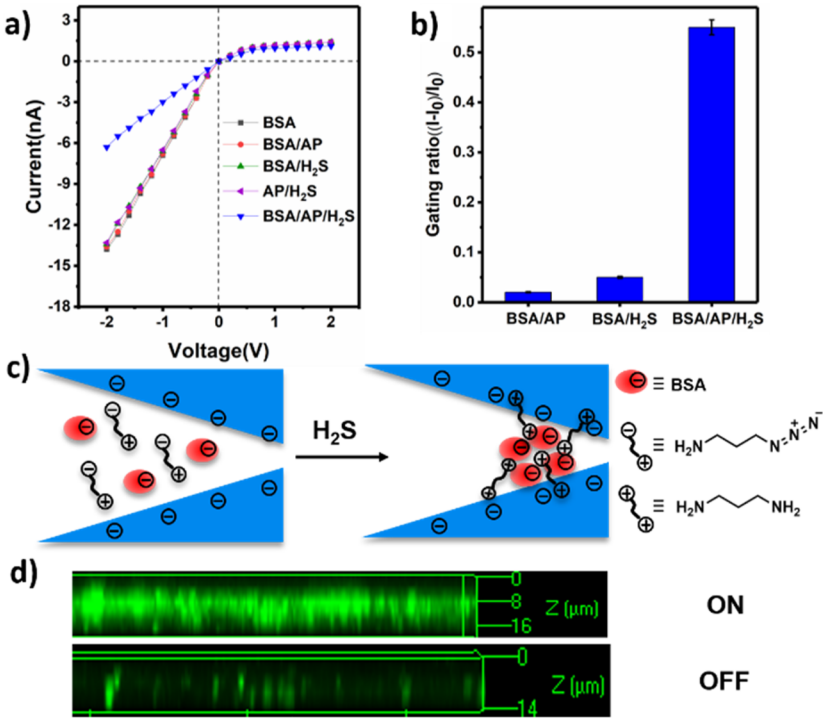

Figure 2. Fabrication of the H_2S-responsive nanochannel biosensor: (a) $I-V$ curves for adding 0.25 mg/mL BSA, BSA/AP, BSA/H_2S, and BSA/AP/H_2S, respectively; (b) current change ratio measured at −2 V; (c) an artificial H_2S-responsive single nanochannel; and (d) the LSCM observation of the BSA fluorescent derivative BSA-FITC complex in the nanochannel.

concentration than bulk solution appeared at negative charged channel, as K^+ enrichment; conversely, K^+ depletion occurred in the positively charged channel. K^+ enrichment owing to EDL overlap at the tip side and a forward concentration gradient owing to K^+ enrichment generated higher ion conductance, as well as a high ion current. In the ON state, the negatively charged channel generates K^+ enrichment, resulting in greater K^+ transport.

RESULTS AND DISCUSSION

To produce the H_2S-reponsive nanodevice biosensor, a single conical nanochannel was fabricated in a polyethylene terephthalate (PET, 12 μm thick) membrane containing a single ion track in the center using the well-developed track-etching technique.[43] The large opening (base) was about 480 nm in size, as observed by scanning electron microscopy (SEM, see Figure S1), while the tip was calculated to be 29 nm in size using an electrochemical method.[44,45] The K^+ transport properties of the label-free nanochannel in response to H_2S were evaluated by measuring current−voltage ($I-V$) curves in phosphate buffered saline (PBS, pH 7.38). As shown in Figure 2a, in the presence of BSA (0.25 mg/mL) or BSA/AP solution, the $I-V$ curves of the bare nanochannel showed an obviously rectified ionic current because of the deprotonation of carboxyl groups on the nanochannel surface under neutral conditions, which can preferentially transport K^+ from the tip entrance to the base side of the channel (ON state). When H_2S was added into this system, only the nanochannel exposed to BSA/AP solution showed a significant decrease in ionic current at −2 V, indicating that K^+ transport through the nanochannel was inhibited (OFF state). Moreover, we also investigated the gating efficiency of this nanodevice regulated by H_2S. H_2S influenced K^+ transport through the nanochannel in terms of a gating ratio, defined as $R_g = (I - I_0)/I_0$, where I_0 and I are the currents measured at −2 V before and after treatment with H_2S. As shown in Figure 2b, in the presence of H_2S, the gating ratio of the nanochannel exposed to BSA/AP solution was significantly higher than that of the control groups. These results were attributed to the azide group of AP in the solution being specifically reduced to an amine by H_2S, with the positive charge of the DP amino group interacting with BSA and leading to decreased stability and electrostatic repulsion of BSA. The resulting formation of BSA agglomerates inhibited K^+ transport through the nanochannel by decreasing both the channel size and the positive charge of the channel surface (Figure 2c). The specific reduction of the azide group of AP by H_2S in the solution was also confirmed by IR spectroscopy (see Figure S2). To verify that H_2S induced the change in BSA charge, we also measured the zeta potential of the PET membrane. At neutral pH values, the zeta potential of the mixture of BSA and AP was about −6.15 mV. When H_2S was added into the solution, the zeta potential increased to +1.94 mV (see Figure S3). SEM images confirmed that many agglomerates appeared in azide/BSA solution after adding H_2S (see Figure S4). Finally, H_2S-induced aggregation of BSA/AP in the nanochannel was tracked by laser scanning confocal microscopy (LSCM). As shown in Figure 2d, a strong fluorescence signal appeared before H_2S addition. However, H_2S reducing the azide led to fluorescein isothiocyanate (FITC) labeled-BSA aggregation, resulting in a dramatic decrease in fluorescence signal.[46]

To verify the high selectivity of the H_2S-responsive nanochannel biosensor, the nanochannel exposed to BSA/AP solution was tested with different substrates (0.1 mM) for 1 min. As shown in Figure 3a, the ion current at −2.0 V drastically decreased from −13.8 to −8.6 nA in the presence of H_2S. In contrast, the ion current was nearly constant in the presence of the other tested substrates, which indicated that

DOI: 10.1021/acs.analchem.9b00752
Anal. Chem. 2019, 91, 6149−6154

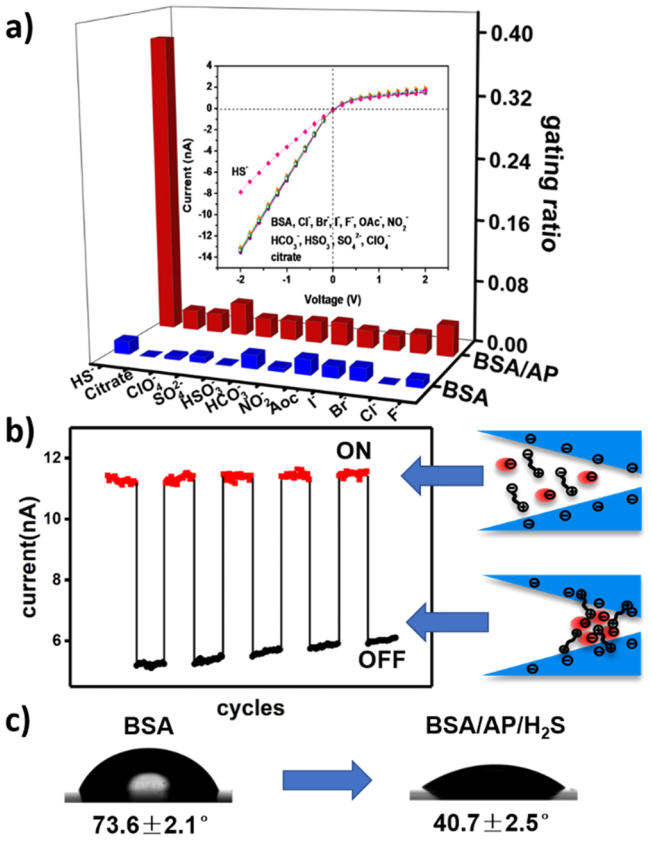

Figure 3. (a) $I-V$ curves and current change ratios measured at −2 V of the single nanochannel biosensor with the addition of 0.25 mg/mL BSA and 5×10^{-5} M AP mixture with 10^{-4} M F^-, Cl^-, Br^-, I^-, OAC^-, NO_2^-, HCO_3^-, HSO_3^-, SO_4^{2-}, ClO_4^-, and citrate respectively. (b) Stability and responsive switch ability of the H_2S-driven ion gate. (c) Photographs of the water droplet shape on the PET films in the absence and presence of H_2S.

the nanochannel biosensor showed high selectivity and specificity for H_2S in the presence of BSA/AP solution. This was attributed to only H_2S specifically reducing the azide group of AP to an amine that can interact with the carboxyl groups ($-COO^-$) of BSA and change the BSA charge, resulting in BSA aggregation. Moreover, the R_g of H_2S (~0.38) was much higher than those of the other substrates, further confirming the high selectivity for H_2S attack (Figure 3a). The ion transport properties of this biosensor were also investigated using current measurements at different H_2S concentrations. The ion current and rectification ratio dramatically decreased with increasing H_2S concentration from 0.3 μM to 1 mM (see Figure S5).

Tunable switching of this ion-gated nanochannel was evaluated by testing the current change with the addition of H_2S in the presence of BSA/AP. As shown in Figure 3b, in the presence of H_2S, the nanochannel surface was hydrophilic and positively charged, which led to a low ion current and high resistance. Under these conditions, the gate was in the OFF state for K^+ selective transport. After regulating the pH to 10, the current at −2 V markedly increased to −13.8 nA owing to DP being removed from the BSA/DP complexes. Besides, the electrostatic repulsion between BSA and channel surface and between BSA agglomerates in solution was also decomposed. Therefore, the nanochannel biosensor changed to negatively charged and hydrophobic, and the gate showed the ON state for K^+ transport. After the process was repeated five times, no damping of the ion current was observed, indicating that this strategy guaranteed the H_2S-responsive nanochannel biosensor with excellent switch ability and stable reversibility. To further verify the progress of the H_2S-responsive biosensor, the wettability of the nanochannels before and after H_2S addition was characterized using contact angle (CA) measurements. As shown in Figure 3c, the wettability of the surface of the nanochannels exposed in BSA/AP led to a marked change before ($67.6 \pm 1.3°$) and after ($40.7 \pm 2.5°$) adding H_2S, corresponding to a change in the chemical composition. On the basis of this promising result, this H_2S-responsive nanochannel biosensor was further applied to complex matrices. With the addition of HS^- and interfering substances (F^-, Cl^-, Br^-, I^-, OAc^-, NO_2^-, HCO_3^-, HSO_3^-, SO_4^{2-}, ClO_4^-, and citrate) at 10^{-4} M in a solution mixture of BSA/AP in 0.1 M PBS (prepared using Yangtze River water) at pH 7.38, H_2S detection still occurred with high selectivity in the real sample (Figure 4a). As shown in Figure 4b, the H_2S dissolved in 0.1 M

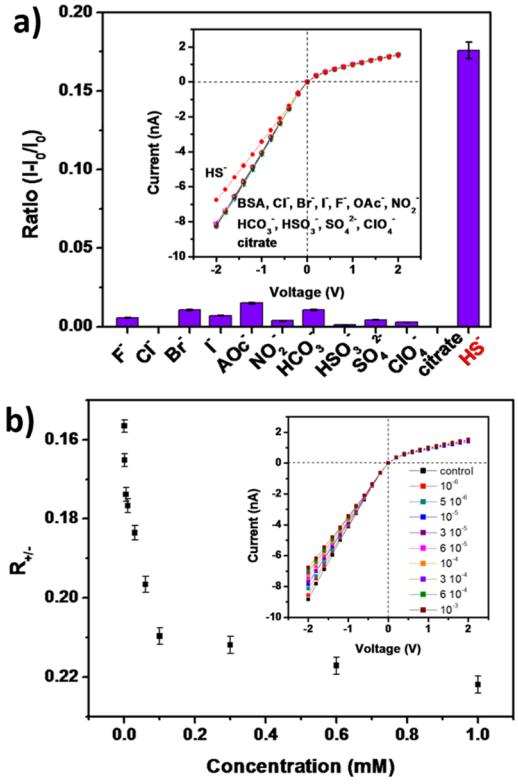

Figure 4. (a) $I-V$ curves and current change ratios measured at −2 V of the single nanochannel with the addition of 0.25 mg/mL BSA/5×10^{-5} M AP, which prepare with actual samples mixture with 10^{-4} M F^-, Cl^-, Br^-, I^-, OAC^-, NO_2^-, HCO_3^-, HSO_3^-, SO_4^{2-}, ClO_4^-, and citrate, respectively. (b) Effect of increasing concentrations of H_2S on the $I-V$ curves and rectification ratios of the label-free single nanochannel in 0.1 mol/L PBS (pH 7.38) with the addition of 5×10^{-7}–7.5×10^{-4} mol/L H_2S (prepare by actual samples).

PBS, which was prepared using Yangtze River water, with the increase in concentration from 1 μM to 1 mM, has obviously changed the ion current and the rectification ratio.

Inspired by the above results, we attempted to elucidate a possible mechanism for H_2S-regulated K^+ transport in the presence of BSA/AP. First, the individual translocation events for BSA in the nanochannel were monitored using chem-clamp

DOI: 10.1021/acs.analchem.9b00752
Anal. Chem. 2019, 91, 6149−6154

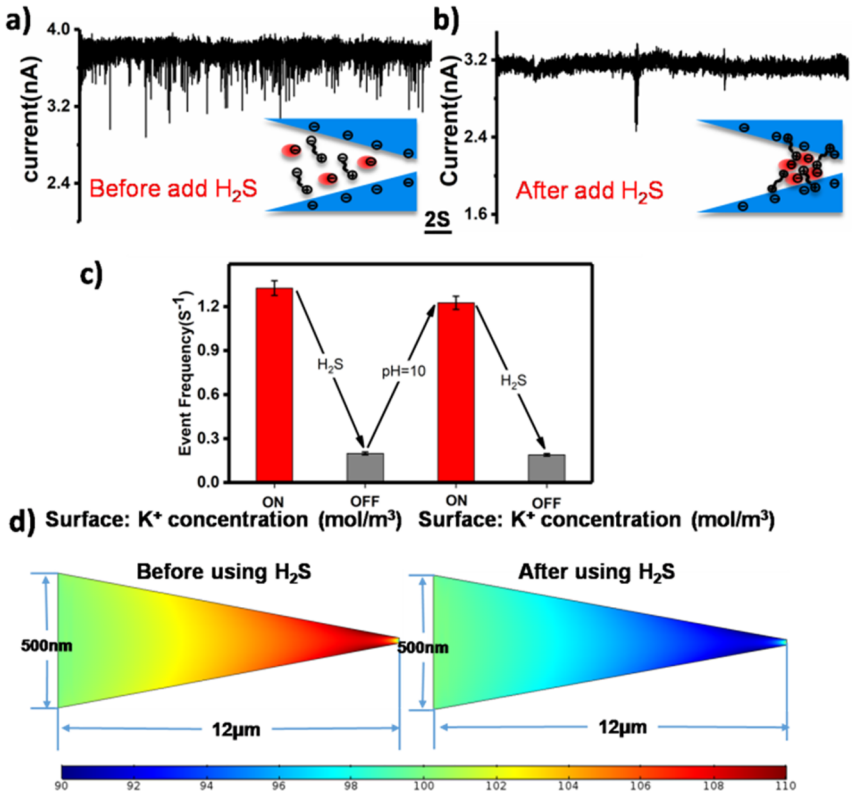

Figure 5. Time dependence of current change during BSA transport in the nanochannel (a) in the absence of H_2S and (b) in the presence of H_2S. (c) The histogram of event counts for BSA transport in the nanochannel over 10 s. Numerical simulation of the nanochannel with varied surface charge: concentration profile of the ion distributions in the nanochannel at +2 V and −2 V: (d) before adding H_2S and after adding H_2S.

technology. As shown in Figure 5a, the ionic current showed an obvious resistive-pulse signature owing to the free state of BSA molecules in the absence of H_2S. However, adding H_2S to the nanochannel generated bits of transient current-block events, which were attributed to the formation of BSA agglomerates (Figure 5b). Moreover, this result could be quantified from event counts over a period of time. Notably, the BSA translocation event rates in the absence of H_2S yielded a frequency of 1.3 events/s, while a frequency of 0.2 events/s was obtained after adding H_2S, which indicated that BSA aggregation efficiently reduced the size of the nanochannel and inhibited K^+ transport (Figure 5c). Moreover, the result shows a reversible and highly robust "OFF" and "ON" switching for K^+ transport based on controlling the BSA aggregation. Finally, finite-element computations based on Poisson and Nernst−Planck (PNP) equations were performed to give theoretical calculation results using COMSOL Multiphysics 5.3.[47] Figure 5d showed the concentration profile obtained from the numerical simulation for a 2D configuration. It is obvious that rather larger concentration than bulk solution appeared at the negatively charged channel, as K^+ enrichment; conversely, K^+ depletion occurred in positively charged channel. The K^+ enrichment resulting from EDL overlap at tip side and, additionally, the forward concentration gradient due to the K^+ enrichment generated higher ionic conductance, as well as a high ion current. Therefore, the H_2S leads to polarity conversion of surface charge, as switching the gate from ON to OFF.

CONCLUSIONS

In summary, a biomimetic H_2S-responsive nanodevice was successfully developed based on an azide reduction reaction controlled BSA aggregation with excellent gating and rectifying properties. This system shows a highly selective response to H_2S, even in complex matrices. Furthermore, this H_2S-responsive biosensor system exhibits excellent reversibility and stability and a fast response rate. These promising results will open a new avenue for better understanding of the synergistic effect of H_2S messengers in ion channels of living organisms and allow its applications in H_2S biosensors and detection.

ASSOCIATED CONTENT

Supporting Information

The Supporting Information is available free of charge on the ACS Publications website at DOI: 10.1021/acs.analchem.9b00752.

SEM, IR, zeta-potential, $I-V$ curve of different concentration in water and actual sample, and calculation of the tip size (PDF)

AUTHOR INFORMATION

Corresponding Authors

*E-mail: sunyaogbasp@mail.ccnu.edu.cn.
*E-mail: lhbing@mail.ccnu.edu.cn.

ORCID

Haibing Li: 0000-0002-6374-4694

Author Contributions

[+]R.Z., X.C., and Z.S. contributed equally to this work.

DOI: 10.1021/acs.analchem.9b00752
Anal. Chem. 2019, 91, 6149−6154

Notes

The authors declare no competing financial interest.

■ ACKNOWLEDGMENTS

This work was supported by grants from the National Key Research and Development Program of China (SQ2018YFD020002), the National Natural Science Foundation of China (21772055, 21572076, 21708012), the Nature Science Foundation of Hubei Province (2018CFB534, 2017CFB151), the 111 Project (B17019), Wuhan Morning Light Plan of Youth Science and Technology (201705304010321), the financial support by self-determined research funds of CCNU from the colleges, Basic Research and Operation of MOE (1100-30106190234). Finally, thanks to the Open Research Fund of Jiangsu Key Laboratory of Medical Optics (JKLMO201803) from Jiangsu Key Laboratory of Medical Optics, Suzhou Institute of Biomedical Engineering and Technology, Chinese Academy of Sciences, Suzhou 215163 (P. R. China).

■ REFERENCES

(1) Szabo, C. *Nat. Rev. Drug Discovery* **2007**, *6*, 917.
(2) Paul, B. D.; Snyder, S. H. *Nat. Rev. Mol. Cell Biol.* **2012**, *13*, 499.
(3) Jiao, X.; Li, Y.; Niu, J.; Xie, X.; Wang, X.; Tang, B. *Anal. Chem.* **2018**, *90*, 533.
(4) Xu, G.; et al. *Angew. Chem., Int. Ed.* **2018**, *57*, 3626.
(5) Fiorucci, S.; Antonelli, E.; Mencarelli, A.; Orlandi, S.; Renga, B.; Rizzo, G.; Distrutti, E.; Shah, V.; Morelli, A. *Hepatology* **2005**, *42*, 539.
(6) Kabil, O.; Banerjee, R. *J. Biol. Chem.* **2010**, *285*, 21903.
(7) Wu, L.; Sun, Y.; Sugimoto, K.; Luo, Z.; Ishigaki, Y.; Pu, K.; Suzuki, T.; Chen, H.; Ye, D. *J. Am. Chem. Soc.* **2018**, *140*, 16340.
(8) Li, Z.; Gong, M.; Xie, H.; Yang, L.; Li, J. *Plant Sci.* **2012**, *185*, 185.
(9) Lai, D.; Mao, Y.; Zhou, H.; Li, F.; Wu, M.; Zhang, J.; He, Z.; Cui, W.; Xie, Y. *Plant Sci.* **2014**, *225*, 117.
(10) Wang, M.; Min, L.; Hou, X. *Science (Shanghai Scientific and Technical Publishers)* **2017**, *69*, 18.
(11) Hou, X.; Zhang, H.; Jiang, L. *Angew. Chem., Int. Ed.* **2012**, *51*, 5296.
(12) Howorka, S.; Siwy, Z. *Chem. Soc. Rev.* **2009**, *38*, 2360.
(13) Boussouar, I.; Chen, Q.; Chen, X.; Zhang, Y.; Zhang, F.; Tian, D.; White, H. S.; Li, H. *Anal. Chem.* **2017**, *89*, 1110.
(14) Howorka, S.; Siwy, Z. *ACS Nano* **2016**, *10*, 9768.
(15) Zhu, Y.; Zhan, K.; Hou, X. *ACS Nano* **2018**, *12*, 908.
(16) Hou, X.; Guo, W.; Jiang, L. *Chem. Soc. Rev.* **2011**, *40*, 2385.
(17) Zhang, F.; Ma, J.; Sun, Y.; Mei, Y.; Chen, X.; Wang, W.; Li, H. *Anal. Chem.* **2018**, *90*, 8270.
(18) Haywood, D. G.; Saha-Shah, A.; Baker, L. A.; Jacobson, S. C. *Anal. Chem.* **2015**, *87*, 172.
(19) Su, G.; Zhang, M.; Si, W.; Li, Z.; Hou, J. *Angew. Chem., Int. Ed.* **2016**, *55*, 14678.
(20) Li, X.; Zhai, T.; Gao, P.; Cheng, H.; Hou, R.; Lou, X.; Xia, F. *Nat. Commun.* **2018**, *9*, 40.
(21) Sun, Y.; et al. *Nat. Commun.* **2018**, *9*, 2617.
(22) Lin, L.; Yan, J.; Li, J. H. *Anal. Chem.* **2014**, *86*, 10546.
(23) Chen, S.; Tang, Y.; Zhan, K.; Sun, D.; Hou, X. *Nano Today* **2018**, *20*, 84.
(24) Ding, D.; Gao, P.; Ma, Q.; Wang, D.; Xia, F. *Small* **2019**, 1804878.
(25) Ali, M.; Yameen, B.; Cervera, J.; Ramirez, P.; Neumann, R.; Ensinger, W.; Knoll, W.; Azzaroni, O. *J. Am. Chem. Soc.* **2010**, *132*, 8338.
(26) Lin, L.; Liu, Y.; Yan, J.; Wang, X. S.; Li, J. H. *Anal. Chem.* **2013**, *85*, 334.
(27) Ali, M.; Neumann, R.; Ensinger, W. *ACS Nano* **2010**, *4*, 7267.
(28) Sun, Y.; Ma, J.; Zhang, F.; Zhu, F.; Mei, Y.; Liu, L.; Tian, D.; Li, H. *Nat. Commun.* **2017**, *8*, 260.
(29) Zhang, F.; Sun, Y.; Tian, D.; Li, H. *Angew. Chem., Int. Ed.* **2017**, *56*, 7186.
(30) Gao, P.; Ma, Q.; Ding, D.; Wang, D.; Lou, X.; Zhai, T.; Xia, F. *Nat. Commun.* **2018**, *9*, 4557.
(31) Sun, Y.; Chen, S.; Chen, X.; Xu, Y.; Zhang, S.; Ouyang, Q.; Yang, G.; Li, H. *Nat. Commun.* **2019**, *10*, 1323.
(32) Wang, H.; Liu, Q.; Li, W.; Wen, L.; Zheng, D.; Bo, Z.; Jiang, L. *ACS Nano* **2016**, *10*, 3606.
(33) Gao, P.; Hu, L.; Liu, N.; Yang, Z.; Lou, X.; Zhai, T.; Li, H.; Xia, F. *Adv. Mater.* **2016**, *28*, 460.
(34) Wang, R.; Sun, Y.; Zhang, F.; Song, M.; Tian, D.; Li, H. *Angew. Chem., Int. Ed.* **2017**, *56*, 5294.
(35) Perez-Mitta, G.; Albesa, A. G.; Trautmann, C.; Toimil-Molares, M. E.; Azzaroni, O. *Chem. Sci.* **2017**, *8*, 890.
(36) Long, Z.; Zhan, S.; Gao, P.; Wang, Y.; Lou, X.; Xia, F. *Anal. Chem.* **2018**, *90*, 577.
(37) Zhang, Z.; Wen, L.; Jiang, L. *Chem. Soc. Rev.* **2018**, *47*, 322.
(38) Wang, M.; Meng, H.; Wang, D.; Yin, Y.; Stroeve, P.; Zhang, Y.; Sheng, Z.; Chen, B.; Zhan, K.; Hou, X. *Adv. Mater.* **2019**, *31*, e1805130.
(39) Sun, Y.; Zhang, F.; Sun, Z.; Song, M.; Tian, D.; Li, H. *Chem. - Eur. J.* **2016**, *22*, 4355.
(40) Zhao, X.; Wang, S.; Younis, M. R.; Xia, X.; Wang, C. *Anal. Chem.* **2018**, *90*, 896.
(41) Peng, H.; Cheng, Y.; Dai, C.; King, A. L.; Predmore, B. L.; Lefer, D. J.; Wang, B. H. *Angew. Chem., Int. Ed.* **2011**, *50*, 9672.
(42) Cao, J.; Lopez, R.; Thacker, J. M.; Moon, J. Y.; Jiang, C.; Morris, S. N. S.; Bauer, J. H.; Tao, P.; Mason, R. P.; Lippert, A. R. *Chem. Sci.* **2015**, *6*, 1979.
(43) Hou, X.; Siwy, Z. S.; Ulbricht, M. *Small* **2018**, *14*, 1800908.
(44) Kalman, E. B.; Sudre, O.; Vlassiouk, I.; Siwy, Z. S. *Anal. Bioanal. Chem.* **2009**, *394*, 413.
(45) Lan, W.; Edwards, M. A.; Luo, L.; Perera, R. T.; Wu, X. L.; Martin, C. R.; White, H. S. *Acc. Chem. Res.* **2016**, *49*, 2605.
(46) Fukuda, J.; Khademhosseini, A.; Yeh, J.; Eng, G.; Cheng, J.; Farokhzad, O. C.; Langer, R. *Biomaterials* **2006**, *27*, 1479.
(47) White, H. S.; Bund, A. *Langmuir* **2008**, *24*, 2212.

DOI: 10.1021/acs.analchem.9b00752
Anal. Chem. 2019, 91, 6149−6154